

On corotation torques, horseshoe drag and the possibility of sustained stalled or outward protoplanetary migration

S.-J. Paardekooper* and J.C.B. Papaloizou

DAMTP, University of Cambridge, Wilberforce Road, Cambridge CB3 0WA, United Kingdom

Draft version 8 July 2021

ABSTRACT

We study the torque on low mass protoplanets on fixed circular orbits, embedded in a protoplanetary disc in the isothermal limit. We consider a wide range of surface density distributions including cases where the surface density increases smoothly outwards. We perform both linear disc response calculations and non linear numerical simulations. We consider a large range of viscosities, including the inviscid limit, as well as a range of protoplanet mass ratios, with special emphasis on the coorbital region and the corotation torque acting between disc and protoplanet.

For low mass protoplanets and large viscosity the corotation torque behaves as expected from linear theory. However, when the viscosity becomes small enough to enable horseshoe turns to occur, the linear corotation torque exists only temporarily after insertion of a planet into the disc, being replaced by the horseshoe drag first discussed by Ward. This happens after a time that is equal to the horseshoe libration period reduced by a factor amounting to about twice the disc aspect ratio. This torque scales with the radial gradient of specific vorticity, as does the linear torque, but we find it to be many times larger. If the viscosity is large enough for viscous diffusion across the coorbital region to occur within a libration period, we find that the horseshoe drag may be sustained. If not, the corotation torque saturates leaving only the linear Lindblad torques. As the magnitude of the non linear coorbital torque (horseshoe drag) is always found to be larger than the linear torque, we find that the sign of the total torque may change even for mildly positive surface density gradients. In combination with a kinematic viscosity large enough to keep the torque from saturating, strong sustained deviations from linear theory and outward or stalled migration may occur in such cases.

Key words: planetary systems: formation – planets and satellites: formation.

1 INTRODUCTION

A planet embedded in a gaseous disc is subject to a net torque that gives rise to orbital evolution. Since the discovery of the first hot Jupiter (Mayor & Queloz 1995), planet migration due to interaction with the protoplanetary disc has become a necessary ingredient of planet formation theory. A considerable amount of analytical and numerical work has gone into understanding the disc-planet interactions leading to planet migration (see Papaloizou et al. 2007, for an overview).

Three modes of migration can be distinguished, in most cases leading to migration towards the central star. High mass planets, for which the Hill sphere is larger than the disc scale height, open up deep gaps in the disc, after which migration proceeds on a viscous time

scale (Lin & Papaloizou 1986). For standard disc parameters, planets more massive than Jupiter migrate in this Type II regime (Crida & Morbidelli 2007). Intermediate mass planets, comparable to Saturn, embedded in massive discs may undergo runaway or Type III migration (Masset & Papaloizou 2003), which may be directed inward as well as outward (Pepliński et al. 2008). In this paper, we focus on low mass planets, with masses typical up to a few times the mass of the Earth (M_{\oplus}). Low mass planets excite linear waves in the disc, the action of which leads to Type I migration (Ward 1997). Linear, semi-analytical calculations have resulted in a widely used torque formula (Tanaka et al. 2002, hereafter TTW02) for isothermal discs.

The total torque on an embedded planet can be decomposed in torques due to waves, which are generated at Lindblad resonances and propagate away from the planet, and corotation torques, generated near the orbit of the planet, where material on average corotates with the planet (see

* E-mail: S.Paardekooper@damtp.cam.ac.uk

Goldreich & Tremaine 1979). For low mass planets, the wave torque is usually thought to dominate the total torque, and, being relatively insensitive to background gradients, lead to inward migration.

Although Type I migration was thought to be mathematically well-understood, it nevertheless posed a serious problem for planet formation. Applying the torque formula from TTW02 (see also Korycansky & Pollack 1993, hereafter KP93) to planets of a few M_{\oplus} embedded in a typical disc resulted in inward migration time scales that are much shorter than the lifetime of the disc. In other words, these planets would all migrate to very small orbital radii, or even into the central star (Ward 1997). Since gaseous giant planets are thought to form around a solid core that is in this mass range, Type I migration theory essentially predicts that there should be no planets at large radii. This has led to investigations on how to slow down or stop Type I migration, for example through the action of magnetic fields (Terquem 2003; Nelson & Papaloizou 2004) or sharp surface density gradients (Masset et al. 2006).

More recently, efforts have been made to relax the isothermal assumption that was made in previous works, and to properly account for the energy budget of the disc. Since radiation is the dominant cooling agent, radiation-hydrodynamical simulations are needed. The outcome of these simulations were surprising: Paardekooper & Mellema (2006a) found that the torque on the planet was *positive*, leading to outward migration, whenever the opacity of the disc at the location of the planet was high enough to make cooling inefficient. In Paardekooper & Mellema (2008) it was recognised that this positive torque was a corotation effect, related to a radial entropy gradient in the unperturbed disc. Baruteau & Masset (2008), through a linear analysis of the corotation torque, suggested that the linear corotation torque in the presence of an entropy gradient can be strong enough to overcome the negative wave torque. However, Paardekooper & Papaloizou (2008) showed that this linear contribution is small, and that a genuinely non-linear effect is responsible for the change of sign of the total torque.

In this paper, we take a step back and reanalyse the isothermal case, in a two-dimensional set-up. The simplicity of this model allows us to perform numerical simulations with high enough resolution investigate in detail non-linear effects on the corotation torque and to run them for long enough to study its possible saturation. We will show that linear theory only applies for short times on the order of a few orbits when a protoplanet is inserted into a disc for which the viscosity is not too large and there is a non-zero corotation torque. We also show that it is a non-linear effect associated with horseshoe bends (Ward 1991) that results in a departure from linear theory. This departure is found to result in torques that can have a much larger magnitude than the linear ones. As the torque scales with the gradient of specific vorticity, this may produce noticeable effects that may even lead to stalled or outward migration, when this gradient is relatively large as for example occurs when the surface density increases gently outwards. For these effects to be sustained the viscosity must be large enough to prevent torque saturation. Viscosities comparable to those often assumed in protoplanetary disc modelling are found to be large enough to enable these non linear corotation torques to be sustained for protoplanets in the Earth mass range.

The plan of the paper is as follows. We start in Section 2 by reviewing the model used throughout the paper. In Section 3, we review and discuss linear corotation torque estimates as well as torque estimates based on the horseshoe drag experienced by material executing horseshoe turns. These are shown to be distinct phenomena with different dependencies on the physical variables, the horseshoe drag being essentially non linear even though the associated torque scales in the same way as the linear one. We go on to perform detailed linear calculations in Section 4, and then compare the linear and non-linear (horseshoe drag) torques in Section 5. In Section 6, we present the results of numerical hydrodynamical simulations, torques are also compared to linear and horseshoe drag estimates confirming the view outlined above. The horseshoe drag is found to be significantly larger than the linear corotation torque and potentially a very important contributor to the total torque for disc surface densities that increase even mildly outwards. We go on to consider the long term torque evolution and saturation as a function of viscosity finding corotation torque saturation in low viscosity cases and sustained corotation torques when the viscosity is large enough to resupply angular momentum to the coorbital region. We discuss our results further in Section 7. Finally we present a short summary, together with some concluding remarks, in Section 8. In addition we give an analysis and discussion of the time development of the linear corotation torque acting on a planet after immersion into a disc, demonstrating that the characteristic time is the orbital period as was found in the numerical simulations.

2 BASIC EQUATIONS

The evolution of a gaseous disc is governed by the Navier-Stokes equations. We will work in a cylindrical coordinate polar frame (r, φ) , centred on the central star, and we integrate the equations of motion vertically to obtain a two-dimensional problem. We are then left with the continuity equation and two equations of motion:

$$\frac{\partial \Sigma}{\partial t} + \nabla \cdot \Sigma \mathbf{v} = 0 \quad (1)$$

$$\frac{\partial \mathbf{v}}{\partial t} + (\mathbf{v} \cdot \nabla) \mathbf{v} = -\frac{\nabla p}{\Sigma} - \nabla \Phi + \mathbf{f}_{\text{visc}}, \quad (2)$$

where Σ is the surface density, $\mathbf{v} = (v, r\Omega)^T$ is the velocity, p is the vertically integrated pressure, Φ is the gravitational potential and \mathbf{f}_{visc} represents the viscous force. We use a locally isothermal equation of state, $p = c_s^2 \Sigma$, where the sound speed c_s may be a prescribed function of radius. We take c_s^2 to be a power law with index $-\beta$, which makes $-\beta$ basically the power law index of the radial temperature profile. Writing $c_s = H\Omega_K$, where H is the vertical pressure scale height and Ω_K is the Keplerian angular velocity, we usually adopt either a sound speed that gives rise to a constant aspect ratio $h = H/r$ (or, equivalently, $\beta = 1$), or a purely isothermal disc with constant c_s ($\beta = 0$). In the latter case, we usually quote the aspect ratio at the location of the planet, $h_p = c_s/(r_p\Omega_p)$. The initial, or for linear calculations the background, surface density is taken to be a power law with index $-\alpha$. Thus $\Sigma = \Sigma_p(r/r_p)^{-\alpha}$, where Σ_p is the surface density at the location of the planet. The gravitational potential Φ is the sum of the potential due to the central star,

the planet's potential Φ_p , and an indirect term that arises due to the acceleration of the coordinate frame centred on the star. For Φ_p , we use a softened point mass potential:

$$\Phi_p = -\frac{GM_p}{\sqrt{r^2 - 2rr_p \cos(\varphi - \varphi_p) + r_p^2 + b^2 r_p^2}}, \quad (3)$$

where G is the gravitational constant, M_p is the mass of the planet, and (r_p, φ_p) are the coordinates of the planet. We will also use q to indicate the mass ratio M_p/M_* , where M_* is the mass of the central star. The softening parameter b should be a sizeable fraction of h , in order to approximate the result of appropriate vertical averaging of the potential.

The exact form of the viscous terms can be found elsewhere (e.g. D'Angelo et al. 2002). We take the kinematic viscosity ν to be a power law in radius, such that the initial surface density profile is a stationary solution. It is easy to see that the required viscosity law is $\nu \propto r^{\alpha-1/2}$. This way, we can neglect a global radial velocity field in the model, which greatly simplifies the analysis. Values quoted in the text refer to ν at the location of the planet, and will be in units of $r_p^2 \Omega_p$, where Ω_p is the angular velocity of the planet.

3 COROTATION TORQUES

The wave (or Lindblad) torque exerted by a low-mass planet on a gaseous disc is relatively well-understood (Goldreich & Tremaine 1979, TTW02). When the Hill sphere of the planet is much smaller than the scale height of the disc, the density waves are excited at Lindblad resonances are linear and the resulting torque can be calculated by performing a linear response calculation and then summing the contributions arising from individual Fourier components (TTW02). This torque usually leads to inward migration, and has been thought to dominate in the Type I regime of low mass planets. There are two approaches that can be followed in order to obtain corotation torques. The first, which we will refer to as the linear estimate, is based on a linear response calculation. The second is a fundamentally different approach based on a direct torque calculation made after making some assumptions about the trajectories of the disc fluid elements, which we refer to as a horseshoe drag calculation. The first approach applies at early times after a protoplanet is inserted into a disc as, at least for a low mass protoplanet, the response must first of all be linear. The second approach applies at later times after the stream-line pattern has adjusted to the presence of the planet.

3.1 Formula for the linear corotation torque for each azimuthal mode number

In order to obtain linear estimates for corotation torques, the equations are linearised (see Section 4) and Fourier-decomposed in azimuth. The resulting single second-order equation (see Goldreich & Tremaine 1979) governing the disc response can be solved to find the corotation torque acting on the planet. Using an approximation scheme that assumes the perturbing potential varies on a scale significantly longer than the scale height, Goldreich & Tremaine (1979) find this torque given by

$$\Gamma_{c,m} = -\frac{m\pi^2 \Phi'_m{}^2}{2d\Omega/dr} \frac{d}{dr} \left(\frac{\Sigma}{\omega} \right), \quad (4)$$

where Φ'_m is the m -th Fourier component of the planet's potential, m is the azimuthal mode number and ω is the flow vorticity, being equal to $\Omega/2$ in a Keplerian disc. All quantities in equation (4) should be evaluated at corotation ($r = r_p$), which makes the total torque proportional to the radial gradient in specific vorticity, or vortensity, in the unperturbed flow there. Of course unless the softening parameter is rather large, the perturbing potential does not vary slowly on the corotation circle and so (4) cannot be used as described above. However, it becomes valid if the perturbing potential Φ'_m is replaced by the generalised potential obtained by adding the enthalpy perturbation to it (see e.g. Lai & Zhang 2006, and the appendix). But then the linear response equations need to be solved in order to determine the enthalpy perturbation in order to evaluate torques using the modified form of (4), which are nonetheless still proportional to the gradient of specific vorticity.

3.2 The total linear corotation torque in the limit of zero softening

To obtain the total torque, one needs to sum the contributions from all values of m (see Ward 1989). For a Keplerian disc with zero softening, the total torque has been calculated, by finding the linear response numerically, to be given by (see TTW02)

$$\Gamma_{c,\text{lin}} = 1.36 \left(\frac{3}{2} - \alpha \right) \frac{q^2}{h_p^2} \Sigma_p r_p^4 \Omega_p. \quad (5)$$

For a 3D disc it is found that the same expression holds but with the numerical coefficient being replaced by 0.632.

An important issue is the time required to develop the linear corotation torque. Being linear this should not depend on the mass of the protoplanet but only on intrinsic disc parameters. Furthermore when a protoplanet is inserted into a disc, there has to be an initial linear phase and for sufficiently low protoplanet mass, the full linear response should develop. As it is somewhat involved, we relegate the discussion of the time development of the linear corotation torque to the Appendix. From this discussion, the characteristic development time is expected to be on the order of the orbital period. We now go on to consider the subsequent development of the corotational flow.

3.3 The horseshoe drag

Ward (1991) derived a formula for the corotation torque using a fundamentally different approach. The argument was based on the expected form of the gas streamlines. These can be classified into four groups as viewed in a reference frame corotating with the planet (see Fig. 1). The first pass the protoplanet interior to the coorbital region and the second pass it exterior to the coorbital region. These groups extend to large distances from the protoplanet. The other two groups consist of material in the corotation region on horseshoe orbits that execute turns close to the planet. The third group approach and leave the protoplanet from its leading side while the fourth do so from its trailing side. These groups are separated by two separatrices (see e.g., Masset et al. 2006; Paardekooper & Papaloizou 2008, for more discussion of this aspect). For low mass protoplanets, most of the corotation torque is produced in a region

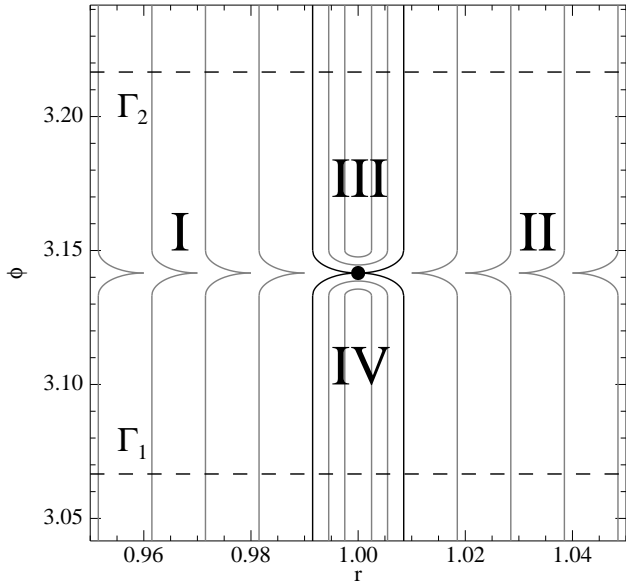


Figure 1. Schematic overview of the horseshoe region, with the planet denoted by the black circle. Solid grey lines indicate approximate streamlines, with the separatrices in black. The separatrices divide the region into four parts, labelled by Roman numerals: I and II, the inner and the outer disc, respectively, and III and IV the leading and trailing part of the horseshoe region, respectively. Two horizontal dashed lines indicate the boundaries of the torque calculation, Γ_1 and Γ_2 . Note that in this figure, the location of Γ_1 and Γ_2 is chosen arbitrarily. In the model, they are chosen to be far enough from the planet so that the corotation torque is determined within.

close to the planet with a length scale expected to be the larger of br_p or H . It is important to note that it takes some time for the streamline structure described above to develop on this scale after insertion of a protoplanet into a disc. As this structure represents a finite deviation from the initial form, this time depends on the mass of the protoplanet. The calculation of the horseshoe drag applies to the situation when this streamline structure has developed on this scale. It is important to note that the time required is shorter than that required to develop it on a scale comparable to r_p which is when issues of torque saturation need to be considered.

Following Ward (1991) we consider the torque produced by material on streamlines undergoing horseshoe turns. We consider a region \mathcal{R} interior to the two separatrices separating these from the first and fourth group of streamlines that is bounded by two lines of constant φ , Γ_1 and Γ_2 on the trailing and leading sides of the protoplanet respectively (see Fig. 1). These boundaries are supposed to be sufficiently far from the protoplanet that the corotation torque is determined within. Assuming a steady state this torque may be obtained by considering the conservation of angular momentum within \mathcal{R} written in the form

$$\Gamma_{c,hs} = \int_{\mathcal{R}} \Sigma \left(\frac{\partial \Phi_{GP}}{\partial \varphi} \right) r d\varphi dr = - \left[\int \Sigma (j - j_p) (\Omega - \Omega_p) r dr \right]_{\Gamma_1}^{\Gamma_2}. \quad (6)$$

Here $j = rv_\varphi$ is the specific angular momentum and j_p is j evaluated at the orbital radius of the protoplanet.

We now follow Ward (1991) and assume the streamline pattern is symmetric on the leading and trailing sides such that a streamline entering on Γ_2 can be identified with a corresponding streamline leaving on Γ_1 at the same radial location. But note that on account of the horseshoe turns, these streamlines will enter \mathcal{R} at different radii. Since, in the barotropic case, potential vorticity or vortensity Σ/ω is conserved along streamlines, and these streamlines are disconnected, this will differ on them. Accordingly we write the torque as

$$\Gamma_{c,hs} = - \int_{\Gamma_2} \Delta \left(\frac{\Sigma}{\omega} \right) \omega (j - j_p) (\Omega - \Omega_p) r dr. \quad (7)$$

Here

$$\Delta \left(\frac{\Sigma}{\omega} \right) = 2 \left(\frac{\Sigma}{\omega} - \frac{\Sigma_p}{\omega_p} \right) \quad (8)$$

is the vortensity difference on the corresponding streamlines which have been assumed to enter \mathcal{R} at the same radial distance from the planet on opposite sides, $\omega_p = \Omega_p/2$ is the vorticity at the planets orbital radius and we have assumed the vortensity to be an even function of radial distance from the protoplanet.

The above integral is easily done if one adopts a first order Taylor expansion for the quantities in brackets and integrates from $r_p - x_s r_p$ to $r_p + x_s r_p$ where the dimensionless width of the horseshoe region is x_s . One obtains (Ward 1991):

$$\Gamma_{c,hs} = \frac{3}{4} \left(\frac{3}{2} - \alpha \right) x_s^4 \Sigma_p r_p^4 \Omega_p^2. \quad (9)$$

Note that as is apparent from the above discussion and that given in the Appendix and also the results of numerical simulations to be presented later, the horseshoe drag, given by equation (9), occurs as a non linear effect that has no counterpart in linear theory (see also Paardekooper & Papaloizou 2008, in addition to Paardekooper & Papaloizou 2009). We also note that numerical hydrodynamical calculations necessarily have $b > 0$, and, two-dimensional simulations, generally adopt $b \approx h$ to account for three-dimensional effects in an approximate way. We will see that this strongly affects the width of the horseshoe region x_s . A detailed analysis of the horseshoe region is presented in Paardekooper & Papaloizou (2009). Here, we adopt a simple estimate for x_s that has proved to be reasonable for smoothing lengths comparable to h_p (Paardekooper & Papaloizou 2008):

$$x_s = \sqrt{\frac{2q}{3b}}. \quad (10)$$

In general, this dependence is to be expected when the separatrix streamline passes through the location of the planet with b possibly being replaced by h_p for small softening (see also Masset et al. 2006). We will compare the horseshoe drag resulting from x_s to the linear corotation torque in Section 5. Note that, since $\Gamma_{c,hs}$ is proportional to x_s^4 , the horseshoe drag would then be proportional to q^2/h_p^2 in the small softening case and q^2/b^2 in the large softening case, just as

$\Gamma_{c,\text{lin}}$. This means that the dependence of the total torque on q , b and h_p would not be a good indication of linearity, since both the linear and the non-linear corotation torque scale in the same way. The only ways to distinguish these are through their magnitudes, and by their time evolution.

The linear corotation torque is set up in approximately an orbital time scale (see the Appendix), similar to the wave torque. This means that, when the background state of the disc is stationary, any evolution in the torque after a few dynamical time scales is due to non-linear effects. The finite width of the horseshoe region gives rise to a *libration* time scale

$$\tau_{\text{lib}} = \frac{8\pi}{3x_s} \Omega_p^{-1}, \quad (11)$$

which is basically the time it takes for a fluid element at orbital radius $r_p(1+x_s)$ to complete two orbits in a frame corotating with the planet. Therefore, this is the time scale on which the corotation torque will saturate due to phase mixing (see Ward 2007), unless some form of viscosity operates on smaller time scales (Masset 2002). Note that saturation is a non-linear process (Ogilvie & Lubow 2003), since it hinges on the finite width of the corotation region.

We will see that there are basically three time scales in the problem, two of which are closely related to non-linearity. First, there is the orbital time scale, on which all linear torques are set up. This is the shortest time scale in the problem. The longest time scale is τ_{lib} , on which saturation operates. A third time scale governs the development of the horseshoe drag, which we will see takes a fraction of a libration time (see also Paardekooper & Papaloizou 2008), and lies in between the time scale for the linear torque development and the saturation time scale.

4 LINEAR CALCULATIONS

Since we are interested in departures from linear theory, it is necessary to first firmly establish what linear theory predicts. The 2D linear calculations of KP93 and TTW02 use a vanishingly small value for b , and these results are therefore not directly comparable to our hydrodynamical simulations. Our customised linear calculations, as briefly outlined below, with b comparable to h , can be directly compared to hydrodynamical simulations.

4.1 Governing equations

Linearising equations (1) and (2), with $\mathbf{f}_{\text{visc}} = 0$, and assuming a Fourier decomposition such that perturbation quantities are the real part of a sum of terms $\propto \exp(im\varphi - im\Omega_p t)$, $m = 0, 1, 2, \dots$, one obtains the following system of equations (Goldreich & Tremaine 1979) for the corresponding Fourier coefficients,

$$i\bar{\sigma}v'_m - 2\Omega u'_m + \frac{dW'_m}{dr} + \frac{d\Phi'_m}{dr} + \frac{\beta W'_m}{r} = 0, \quad (12)$$

$$i\bar{\sigma}u'_m + 2Bv'_m + \frac{imW'_m}{r} + \frac{im\Phi'_m}{r} = 0, \quad (13)$$

$$\frac{i\bar{\sigma}W'_m}{c_s^2} + \frac{dv'_m}{dr} + (1-\alpha)\frac{v'_m}{r} + \frac{imu'_m}{r} = 0, \quad (14)$$

where primes denote perturbation quantities, and the subscript m , being the azimuthal mode number, indicates the

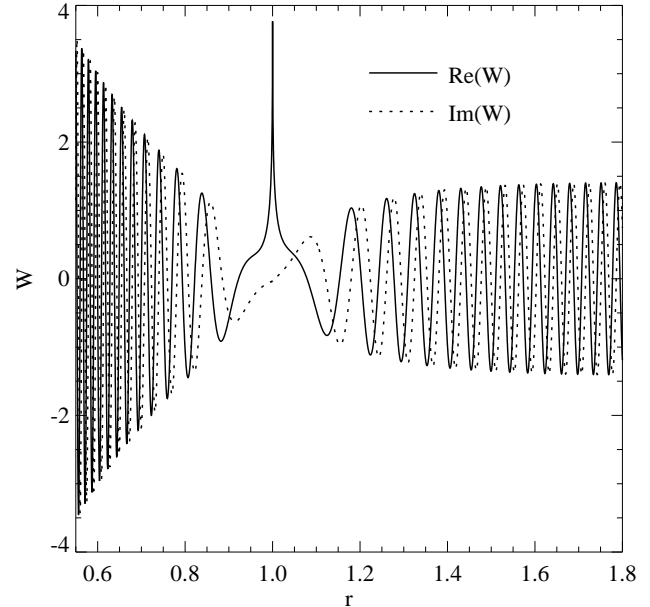


Figure 2. Real (solid) and imaginary (dotted) part of the enthalpy perturbation W , for an isothermal, constant surface density disc with $h_p = 10^{-3/2}$ and a softening parameter as used in KP93 ($b = 10^{-4}$) plotted as a function of radius in units of r_p .

m -th Fourier coefficient. Here the velocity perturbation is $\mathbf{v}'_m = (v'_m, u'_m)$, $W'_m = c_s^2 \Sigma'_m / \Sigma$ is the enthalpy perturbation, $\bar{\sigma} = m(\Omega - \Omega_p)$, B is the second Oort constant, and Φ'_m is the m -th Fourier component of Φ_p , being a real quantity. The term proportional to β is not present in the equations of KP93, because they considered a strictly barotropic equation of state. Eliminating u_m , we obtain a system of ordinary differential equations (KP93):

$$\frac{dv'_m}{dr} = - \left(1 - \alpha - \frac{2mB}{\bar{\sigma}} \right) \frac{v'_m}{r} + i \left(\frac{m^2}{\bar{\sigma}r^2} - \frac{\bar{\sigma}}{c_s^2} \right) W'_m + \frac{im^2\Phi'_m}{\bar{\sigma}r^2} \quad (15)$$

$$\frac{dW'_m}{dr} = -i \left(\frac{\bar{\sigma}^2 - \kappa^2}{\bar{\sigma}} \right) v'_m - \frac{2m\Omega(W'_m + \Phi'_m)}{\bar{\sigma}r} - \frac{d\Phi'_m}{dr} - \frac{\beta W'_m}{r}, \quad (16)$$

where $\kappa^2 = 4B\Omega$ is the square of the epicyclic frequency.

We have solved equations (15) and (16) using a sixth order Runge-Kutta method and outgoing wave boundary conditions (see KP93). In Fig. 2, we show the resulting W'_m for $m = 10$, for an isothermal, constant surface density disc with $h_p = 10^{-3/2}$ and a very low value of the softening parameter $b = 10^{-4}$. The same case was shown in KP93 (their figure 2), and the results agree very well.

The imaginary part of W'_m is directly related to the torque density:

$$\frac{d\Gamma_m}{dr} = \pi m \Phi'_m \Sigma \frac{\mathcal{I}m(W'_m)}{c_s^2}, \quad (17)$$

and the total torque on the planet Γ_m can be found by integrating over the whole disc. Goldreich & Tremaine (1979) showed that the Lindblad torque is carried away by density

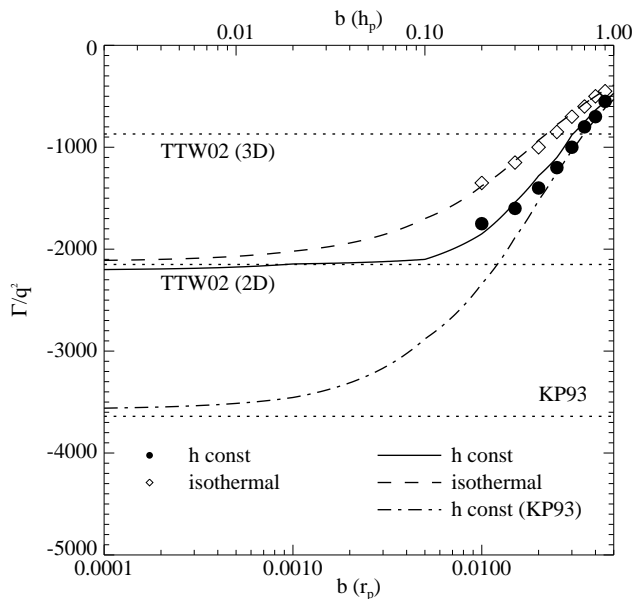


Figure 3. Total torque on the planet, obtained from linear calculations, as a function of the softening parameter b . The surface density is proportional to $r^{-3/2}$ ($\alpha = 3/2$), which means that the corotation torque vanishes in the barotropic case. The disc is either fully isothermal with $h_p = 0.05$ (dashed line) or has a constant aspect ratio $h = 0.05$ (solid line). Calculations similar to those of KP93 with constant h are indicated by the dash-dotted line. Also shown are the results of linear calculations in 2D by KP93 (for constant h) and the isothermal results of TTW02, for 2D as well as 3D. Both 2D studies used a very small (KP93) or vanishing (TTW02) softening length. Filled circles denote the torques measured from hydrodynamical simulations for a $q = 1.26 \cdot 10^{-5}$ planet in a disc with constant h , and diamonds the results for isothermal simulations with $h_p = 0.05$.

waves, resulting in an angular momentum flux

$$F_m = -\frac{m\pi r \Sigma}{\bar{\sigma}^2 - \kappa^2} \left[\mathcal{I}m(W'_m) \frac{d}{dr} (\mathcal{R}e(W'_m) + \Phi'_m) - (\mathcal{R}e(W'_m) + \Phi'_m) \frac{d\mathcal{I}m(W'_m)}{dr} \right]. \quad (18)$$

Therefore, the Lindblad torque is given by $\Delta F_m = F_m(r_{\text{out}}) - F_m(r_{\text{in}})$, where r_{in} and r_{out} denote the inner and the outer radius of the disc, respectively. We can therefore calculate the corotation torque as (KP93):

$$\Gamma_{c,m} = \Gamma_m - \Delta F_m, \quad (19)$$

and the total torques can be found by summation over all m .

4.2 Results

We start by considering a disc with constant specific vorticity, which means that the corotation torque vanishes. This allows us to look in some more detail at the Lindblad torque alone. In Fig. 3, we show the total torque¹ for three different cases: strictly isothermal (dashed line), locally isother-

¹ In all figures, the torque is given in units of $\Sigma_p r_p^4 \Omega_p^2$, and is divided by q^2 to make it independent of the mass of the planet.

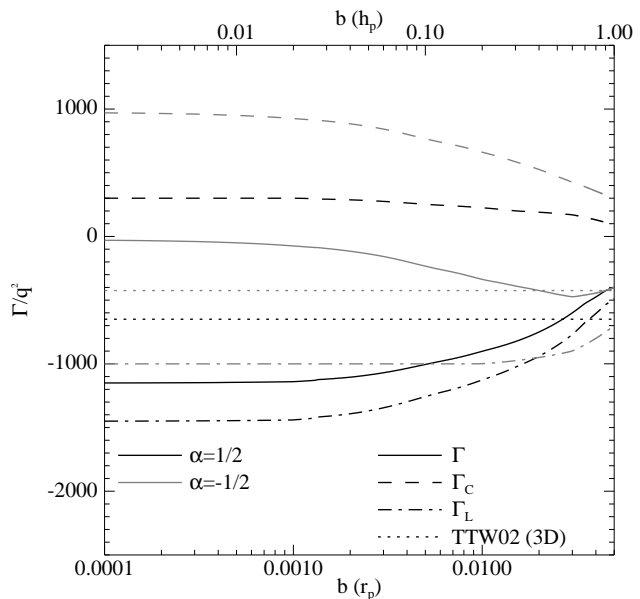


Figure 4. Lindblad (dash-dotted curves) and corotation (dashed curves) torques obtained from an isothermal ($h_p = 0.05$) linear calculation as a function of softening parameter b for two different density profiles. Black curves: $\alpha = 1/2$, grey curves: $\alpha = -1/2$. The solid curves denote the total torques, and the horizontal dotted lines the 3D results of TTW02.

mal (h constant; solid line) and locally isothermal without the term proportional to β in equation (12) (dash-dotted line). The latter case is similar to the one considered in KP93, and approaches the result of KP93 for small softening. Similarly, the strictly isothermal case approaches the 2D result of TTW02 for small softening. For appropriate values of $b \approx h$, differences between the strictly and locally isothermal models can be as large as 30%. In the remainder of this paper, we will restrict ourselves to the strictly isothermal equation of state, since the horseshoe drag has been analysed for barotropic fluids only (Ward 1991)². For this case, a smoothing length of $b = 0.025$, corresponding to $0.5 h$, results in the total torque being equal to the 3D calculations of TTW02.

We now introduce a corotation torque in the calculations by considering different values of α . In Fig. 4, we show the linear Lindblad and corotation torques for $\alpha = 1/2$ and $\alpha = -1/2$. Note that in the latter case, the surface density gradient is positive, which may be unrealistic except for special locations in the disc (see for example Masset et al. 2006), but it serves as a good example of a case with strong corotation torques. For $\alpha = 1/2$, the corotation torque is much smaller than the Lindblad torque, and is increased by a factor of 3 going from $b = h$ to $b = 0$, similar to the Lindblad torque. Therefore, the corotation torque is a small fraction of the Lindblad torque for all values of b considered here. That is not the case for $\alpha = -1/2$, where for small soft-

² In Paardekooper & Papaloizou (2008), horseshoe drag was studied in adiabatic flows, where entropy (but not vortensity) is conserved. For a locally isothermal equation of state, neither of these is conserved, with the consequence that it is unclear what the horseshoe drag is in this case.

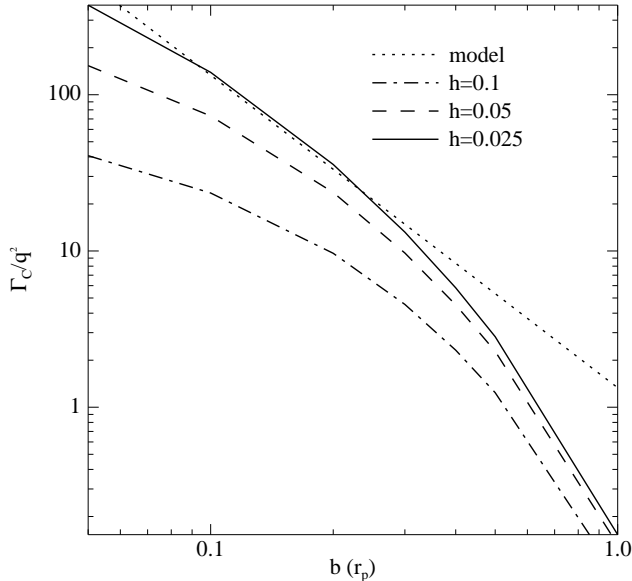


Figure 5. Corotation torque, obtained from a linear calculation with $\alpha = 1/2$ and $h_p = 0.025$ (solid line), $h_p = 0.05$ (dashed line), and $h_p = 0.1$ (dash-dotted line). The dotted line gives the prediction of equation 24, valid for $h \ll b \ll 1$.

ening parameters the corotation torque is almost the same as the Lindblad torque. The sign of the total torque will change for $\alpha < -1/2$, which is expected from the 2D results of KP93 and TTW02. For 3D calculations, the situation is different (TTW02), which is illustrated by the results in Fig. 4 for larger softening. For all values of α considered in Figs. 3 and 4 we find that for a softening length of $b = 0.5 h$ we can match our 2D calculations with the 3D work of TTW02.

4.3 The limit of large softening

We now relate our numerical results to the predictions made using the torque formula (4) given by Goldreich & Tremaine (1979). This is applicable to the situation where the softening parameter is significantly larger than the scale height and we use it to evaluate the corotation torque in that limit. To do this we adopt the approximation for Φ'_m introduced by Goldreich & Tremaine (1980) for $m > 0$ in the form

$$\Phi'_m = \frac{1}{\pi} \int_0^{2\pi} \Phi_p \cos(m\varphi) d\varphi \sim -\frac{2}{\pi} \frac{GM_p}{r_p} K_0(m\zeta), \quad (20)$$

where K_0 is the standard Bessel function and

$$\zeta = \sqrt{\frac{(r - r_p)^2}{r_p^2} + b^2}. \quad (21)$$

This is valid in the important domain of interest where $m \sim 1/b$, and $|r_p - r| \ll br_p$. Summing the torques given by (4) over m , using (20) we obtain

$$\sum_{m=1}^{\infty} \Gamma_{c,m} = \left(\frac{3}{2} - \alpha\right) \frac{8q^2}{3} \Sigma_p r_p^4 \Omega_p^2 \sum_{m=1}^{\infty} m K_0(mb)^2, \quad (22)$$

where Σ_p denotes the unperturbed surface density at the planets location. Noting that b is small and that the dominant contribution to the sum on the right hand side comes

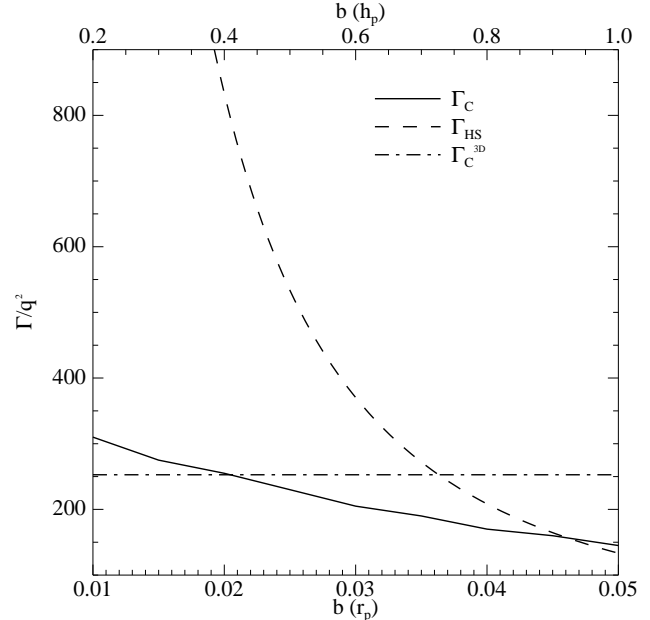


Figure 6. Corotation torque, obtained from a linear calculation with $\alpha = 1/2$ and $h_p = 0.05$ (solid line), together with the horseshoe orbit drag (dashed line) for our simple estimate of the width of the horseshoe region. Also shown is the 3D result of TTW02 (dash-dotted line).

from large $m \sim 1/b$, we replace the sum by an integral, thus

$$\sum_{m=1}^{\infty} m K_0(mb)^2 \rightarrow \left(\frac{1}{b}\right)^2 \int_0^{\infty} x K_0(x)^2 dx = \frac{1}{2} \left(\frac{1}{b}\right)^2. \quad (23)$$

Thus we obtain

$$\sum_{m=1}^{\infty} \Gamma_{c,m} = \Gamma_{c,\text{lin}} = \left(\frac{3}{2} - \alpha\right) \frac{4q^2}{3b^2} \Sigma_p r_p^4 \Omega_p^2. \quad (24)$$

We remark that Ward (1992) obtained a corresponding expression for a vertically averaged potential, that has the same scaling when b is replaced by h_p in the above equation.

A comparison of the torques given by equations (5) and (24) indicates that the effect of softening should be significant for $b \gg 1.4h_p$. But note that in addition to requiring $b/h \gg 1$ (24) also formally requires $b \ll 1$. This means, as we shall see below, that the limit where (24) applies requires rather small $h \ll 0.025$.

We now directly compare linear calculations with the prediction of equation (24). The results are illustrated in Fig. 5, for three different values of h_p . Note that in the derivation of equation (24) it was assumed that $b \ll 1$, so we expect the torque to be given by equation (24) for $h \ll b \ll 1$. From Fig. 5, we see that for $h_p = 0.025$ we can nicely reproduce equation (24) for $0.05 < b < 0.2$. However, as h_p increases there are increasing deviations from equation (24). For $h_p = 0.05$ and $0.1 < b < 0.2$, the maximum and minimum deviations are by a factor of 2 and 1.5 respectively, while for $h_p = 0.1$ the deviation always exceeds a factor of two.

5 A COMPARISON OF THE EXPECTED HORSESHOE DRAG WITH THE LINEAR COROTATION TORQUE

In this section we compare corotation torques obtained from linear calculations to the expected horseshoe drag. We obtain the latter from equation (9) which requires an estimate of x_s which we obtain from equation (10) which simulations have indicated gives a good estimate for $b \sim h_p$. We shall obtain estimates for the horseshoe drag directly from simulations and make further comparisons below.

In Fig. 6, we show the linear corotation torque (solid line), together with the horseshoe drag, obtained as indicated above, (dashed line) for a disc with $\alpha = 1/2$, for different values of the smoothing parameter b . For reasonable values of b , the horseshoe drag is stronger than the linear corotation torque making the torque on the disc more negative. Thus the horseshoe drag on the planet is positive and larger than the linear corotation torque. For smoothing parameters $0.02 < b < 0.03$, this non-linear torque is a factor 2–3 larger than the linear torque. For smaller values of b , equation (10) predicts a value of x_s that is too large and accordingly a horseshoe drag that is too large. In reality we expect both the horseshoe width and therefore the horseshoe drag to reach limiting values for small b and these values should be larger than those we obtain here using values of b for which equation (10) applies. A more complete discussion of these aspects is given in Paardekooper & Papaloizou (2009). Also shown in Fig. 6 is the corotation torque obtained for the corresponding three-dimensional disc (TTW02) which has zero softening. For $b = 0.02$, we can match our 2D linear calculation to the 3D result of TTW02. However, for the same softening the horseshoe drag is three times as large.

For a large softening with $b = 0.7h_p = 0.035$, the horseshoe drag is equal to the 3D unsoftened linear corotation torque. However, numerical results show that for this smoothing length, equation (10) actually slightly underestimates the true value of x_s , with the consequence that the intersection of the horseshoe drag with the 3D linear corotation torque occurs for approximately $b = 0.8h_p$. Lacking a full 3D model of the horseshoe region, it is difficult to say what value of b to choose so that 2D results match 3D results. However, numerical results suggest that $b < 0.02$ may be appropriate (Masset et al. 2006). We come back to this issue in Section 7, but it is good to keep in mind that the effects discussed in the next sections may well be stronger in 3D calculations.

6 HYDRODYNAMICAL SIMULATIONS

In the previous section, we have established that horseshoe drag is potentially much stronger than the linear corotation torque. We now turn to numerical hydrodynamic simulations to show that indeed strong deviations from linear theory are encountered in practice. We use the RODEO method (Paardekooper & Mellema 2006b) in two spatial dimensions, on a regular grid extending from $r = 0.5r_p$ to $r = 1.8r_p$ and which covers the whole 2π in azimuth. Since we want to resolve the horseshoe region for even the smallest planets we consider, a relatively high resolution is required: 1024 cells in the radial and 4096 cells in the azimuthal direction, making the resolution at the location of the planet approximately

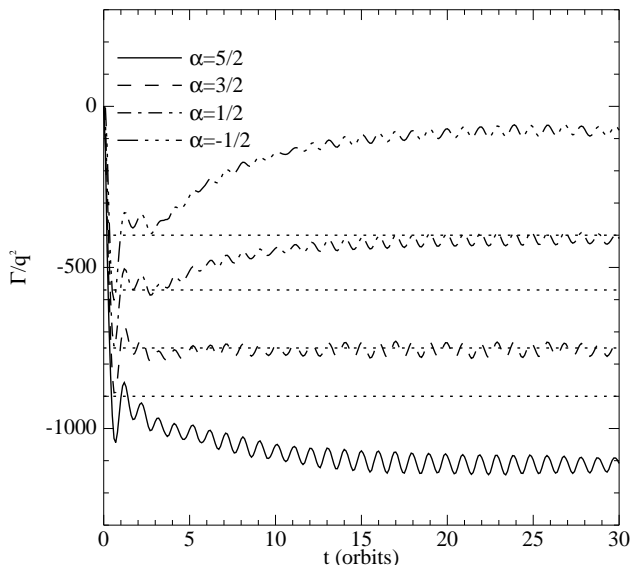


Figure 7. Total torque on the planet for an isothermal, inviscid $h_p = 0.05$ disc with $b = 0.03$ and $q = 1.26 \cdot 10^{-5}$, for different surface density profiles. The dotted lines indicate the linear torque, for increasing α from top to bottom.

$0.0015r_p$ in both directions. Tests have shown that this resolution is sufficient to capture the horseshoe dynamics for $x_s > 0.004$. We include all disc material in the torque calculation (not excluding any material close to the planet), and the planet is introduced with its full mass at $t = 0$. For low mass planets, this does not affect the results.

First, in Section 6.1, we study the development of the horseshoe drag and its relationship to linear theory. Then, in Section 6.2, we study the long-term behaviour (saturation) of the corotation torque.

6.1 Development of the non-linear torque

We start by considering a planet with a relatively high mass, $q = 1.26 \cdot 10^{-5}$, which corresponds to $4 M_{\oplus}$ around a Solar mass star. Although this is the planet with the largest mass we consider, it has been expected to be well within the linear regime (Masset et al. 2006). In Fig. 3, we show that for a disc with constant specific vorticity, we can reproduce the expected linear torque for all reasonable values of b . For very small values of b , one may expect a departure from linear theory, since at this point, an envelope may form that is gravitationally bound to the planet, which probably should be excluded from the torque calculation. We do not consider this regime here, since we expect to adopt a value of b comparable to h in order to account for vertical averaging. The important point is that we can match our linear calculations to the hydrodynamical simulations in the absence of corotation torques (linear as well as non-linear).

This is further illustrated in Fig. 7, where we show the time evolution of the total torque on the planet for different surface density profiles. We see that the case with $\alpha = 3/2$ nicely falls on the corresponding linear result. Note also that this torque is set-up in approximately one orbital period. This is to be expected for both the Lindblad and the linear corotation torque (see the Appendix).

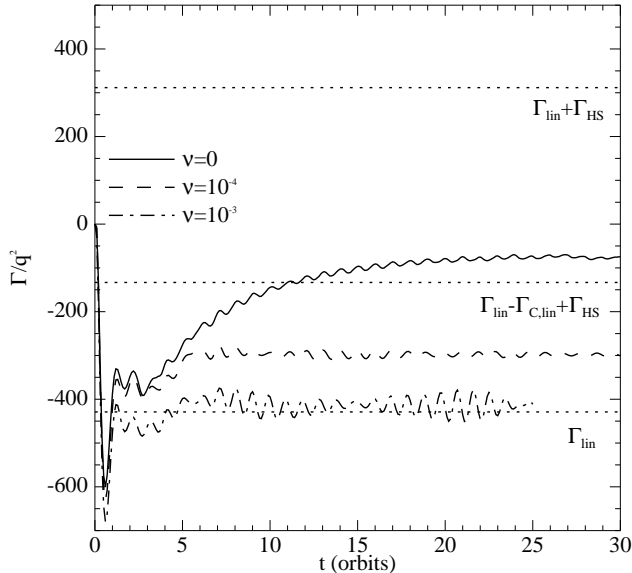


Figure 8. Total torque on the planet in an isothermal $h_p = 0.05$ disc with $\alpha = -1/2$ for $b = 0.03$ and $q = 1.26 \cdot 10^{-5}$ for different magnitudes of the viscosity. The horizontal lines indicate, from bottom to top, the total linear torque, the Lindblad torque with the horseshoe torque (found using the procedure outlined in Section 5) added, and the total linear torque with the horseshoe torque added.

Different surface density profiles give remarkably different results. All cases except $\alpha = 3/2$ show a departure from linear theory, the sign of which is dictated by the vortensity gradient. This indicates that the corotation torque is enhanced with respect to its linear value. This enhancement takes approximately 20 orbits to develop after which the torques attain steady values for the remainder of the simulations. This time period, as we show below, can be understood as being a fraction of the libration time scale, and is therefore related to a non-linear effect. Note that in all cases, linear theory is only valid at early times (less than about two orbits) during which as expected the linear corotation torque is set up on a dynamical time scale. At later times, it gets replaced by the non-linear horseshoe drag.

We take a closer look at the $\alpha = -1/2$ case illustrated in Fig. 8. The horizontal dotted lines indicate, from bottom to top, the linear torque, the linear Lindblad torque with the horseshoe drag added, and the total linear torque with the horseshoe drag added. From the solid line, we see that the total torque can be understood as the linear torque, with the linear corotation torque replaced by the horseshoe drag. We have found this to be true for all values of α considered (see Fig. 9). It is also expected from the discussion given in Section 3.

The magnitude of the non-linear torque depends on the magnitude of the viscosity in the disc. Recall that whenever we include viscosity in the model, we do not allow for large scale mass flow with respect to the planet (see also Section 7). It is easy to understand this dependence, since the horseshoe drag model hinges on vortensity conservation while the fluid executes a horseshoe turn. For strong enough viscosities, we can recover the linear torque, but note that the large values $\nu \gg 10^{-3}$ required correspond to a very

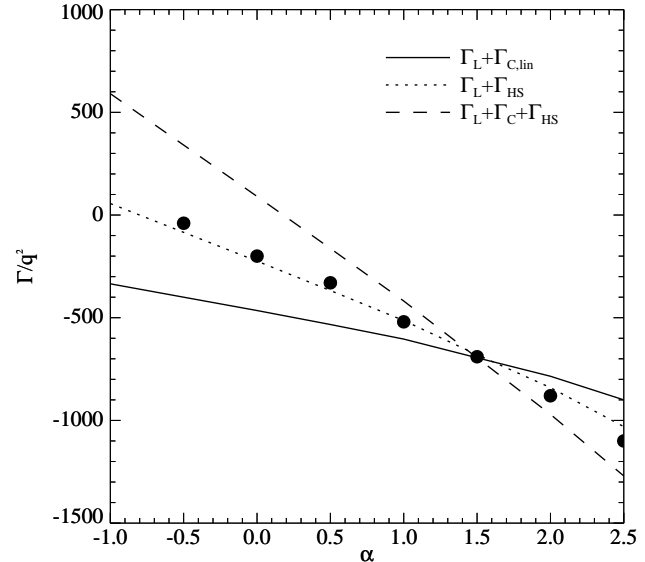


Figure 9. Total torque on a $q = 1.26 \cdot 10^{-5}$ planet embedded in an isothermal $h_p = 0.05$ inviscid disc for $b = 0.03$ after 30 orbits. The solid line indicates the linear torque, and the dashed line shows the total linear torque plus the estimated horseshoe drag. The dotted line indicates the linear Lindblad torque plus the non-linear horseshoe drag. Symbols denote results obtained from hydrodynamical simulations for different values of the surface density power law index α .

large α viscosity parameter of $\alpha_{\text{visc}} = 0.4$. This is because only then can the viscosity directly affect the horseshoe turn. In Section 6.2, we will see that lower viscosities are in fact sufficient to keep the torque unsaturated.

Returning to inviscid discs, we show in Fig. 9 the total torque on the disc for different values of α , confirming that the horseshoe drag indeed replaces the linear corotation torque. Note that we expect a torque reversal around $\alpha = -1$, while the linear calculations predict this would only happen around $\alpha = -3$. Note also that steep density profiles result in an acceleration of inward migration with respect to the linear estimate.

Linear theory predicts that the torque should scale as q^2 . Since in our simple model, the horseshoe width scales as $q^{1/2}$, the non-linear contribution to the torque (the horseshoe drag) also scales as q^2 . Therefore, it could be misinterpreted as a linear effect. However, the time scale on which the horseshoe drag term is set up depends on the mass of the planet. We will see below that it takes a fixed fraction of a libration time scale. This means that although the full non-linear torque scales as q^2 , this will not be the case at intermediate stages. This is illustrated in Fig. 10, where we show the time evolution of the torque for different mass ratios. For linear torques, all curves would fall on top of each other. This is indeed true at early times, when the horseshoe drag has not yet developed. When the horseshoe drag takes over, however, planets of different mass give different results; lower-mass planets take longer to develop the non-linear torque.

If we rescale the time axis to the libration time (see Fig. 11), the curves fall on top of each other again. This is because the time scale to set up the horseshoe drag is a fixed fraction

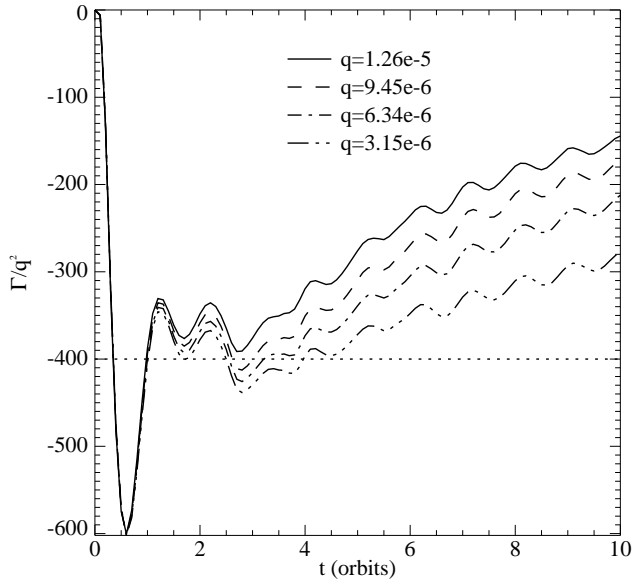


Figure 10. Total torque on a planet in an isothermal $h_p = 0.05$ disc for $b = 0.03$ and $\alpha = -1/2$, for different values of q . The dotted line indicates the linear torque.

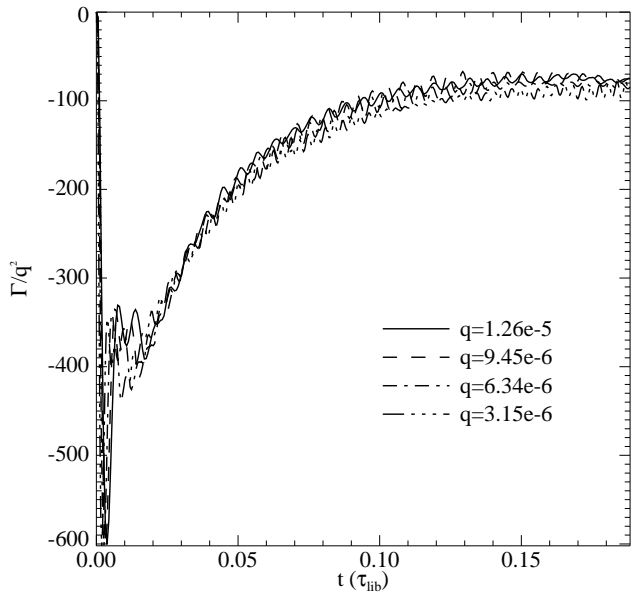


Figure 11. Total torque on the planet embedded in an isothermal $h_p = 0.05$ disc for $b = 0.03$ and $\alpha = -1/2$, for different values of q . The time is in units of τ_{ib} , which scales as $q^{-1/2}$.

of the libration time (approximately 15%, according to Fig. 11). One might expect that, as the scale of the region contributing the torque is of order H , the time required would be on the order of a factor h_p smaller than the libration time. Thus the results presented here are consistent with this time being about $2h_p\tau_{\text{ib}}$. This type of phenomenon was also discussed in Paardekooper & Papaloizou (2008), where it was shown that the development of the non linear torque is due to an high density ridge resulting from material that has

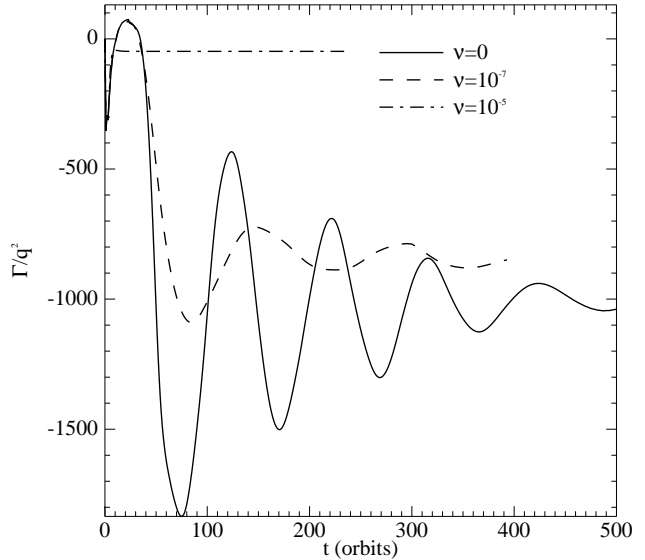


Figure 12. Total torque on a planet in an isothermal $h_p = 0.05$ disc for $q = 1.26 \cdot 10^{-5}$, $b = 0.02$ and $\alpha = -1/2$, for different values of the viscosity ν .

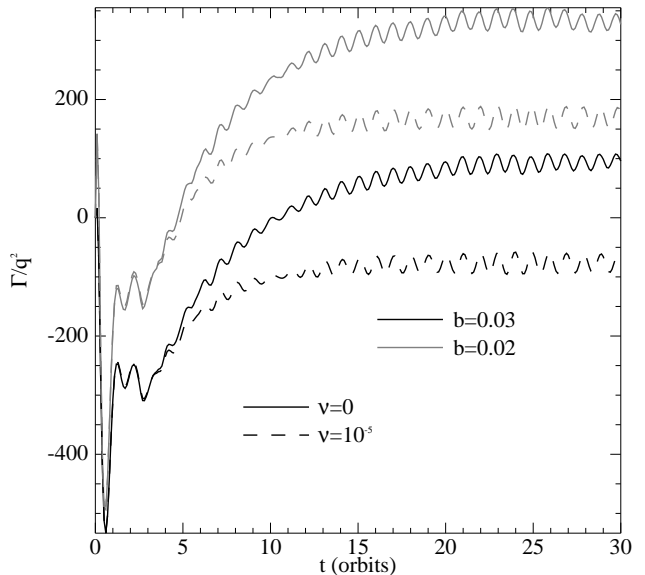


Figure 13. Total torque on a planet in an isothermal $h_p = 0.05$ disc for $q = 1.26 \cdot 10^{-5}$ and $\alpha = -1$, for different values of softening parameter b and viscosity ν .

executed a horseshoe turn at constant entropy (replacing specific vorticity applicable to this case).

6.2 Long-term evolution

Lindblad torques give rise to waves that carry away angular momentum. Therefore, the planet can continue to exchange angular momentum with the disc at Lindblad resonances. However, there is no wave transport in the corotation region, and therefore in the absence of any other form of transport, only a finite amount of angular momentum exchange with the planet can occur before the structure of the coorbital

region is significantly modified. In other words, the corotation region is a closed system unless there is some diffusive process operating in the disc that can transport angular momentum there. In the absence of such diffusion, the corotation torque will saturate (Ogilvie & Lubow 2003).

Saturation is an inherently non-linear process, as it depends again on a finite width of the corotation region. The time scale on which saturation operates is the libration time scale, and diffusion must operate on a smaller time scale in order to prevent saturation. For a viscosity coefficient ν , one needs

$$\nu > \frac{x_s^3}{4} r_p^2 \Omega_p, \quad (25)$$

(see Masset 2002, who considered this process for a disc with constant surface density). For a level of viscosity that has become standard in disc-planet interaction studies, $\nu = 10^{-5} r_p^2 \Omega_p$, all protoplanets considered here are of small enough mass that we expect the corotation torque to be unsaturated. We consider a planet of $q = 1.26 \cdot 10^{-5}$, and use a softening parameter $b = 0.02$ to make the libration time scale as short as possible to ease the computational burden. In Fig. 12, we show the long-term evolution of the torque for three different levels of viscosity. The inviscid case shows strong libration cycles, before the torque starts to settle to a value that is close to the linear Lindblad torque ($\Gamma_L \approx -1000q^2$, see Fig. 4).

A small viscosity of $\nu = 10^{-7}$ gives less prominent libration cycles, and the torque settles at a value of approximately -850 . In this case, corotation torques are partially saturated. This is in quantitative agreement with the analysis of Masset (2001), where it is argued that the horseshoe drag should be multiplied by a factor $\mathcal{F}(z)$ with $z = x_s(2\pi\nu)^{-1/3}$ to account for saturation. Choosing the smallest option for \mathcal{F} given in Masset (2001), which gave the best fit in Masset (2002), we find $\mathcal{F} = 0.114$. This predicts a corotation torque of $\Gamma_C = 125$, while the difference between the Lindblad torque and the total torque as measured from the simulations (the asymptotic difference between the dashed and solid curve in Fig. 12) is 150.

For $\nu = 10^{-5}$ the libration cycles disappear, indicating that the torque remains unsaturated. There is basically no evolution of the torque once the non linear contribution has been set up. This again agrees with the analysis of Masset (2001), where for this value of ν we expect \mathcal{F} close to unity. Note, however, that the maximum torque that can be reached is reduced for this relatively high viscosity (see also Fig. 8).

Finally, we show in Fig. 13 that, for a softening parameter $b = 0.02$, low mass planets will feel a sustained positive torque when $\alpha = -1$, which corresponds to a mildly positive surface density gradient. Although a viscosity $\nu = 10^{-5}$ reduces the non-linear torque, making the torque negative for $b = 0.03$, it is necessary for the torque to be sustained. For a slightly smaller softening parameter, $b = 0.02$, we find sustained outward migration. Note that from Figs. 3 and 4 we expect a smoothing around $b = 0.025$ to reproduce 3D effects. Full 3D simulations, together with a 3D understanding of horseshoe dynamics, are needed to see how this non-linear torque behaves in a three-dimensional setting (see also Section 7).

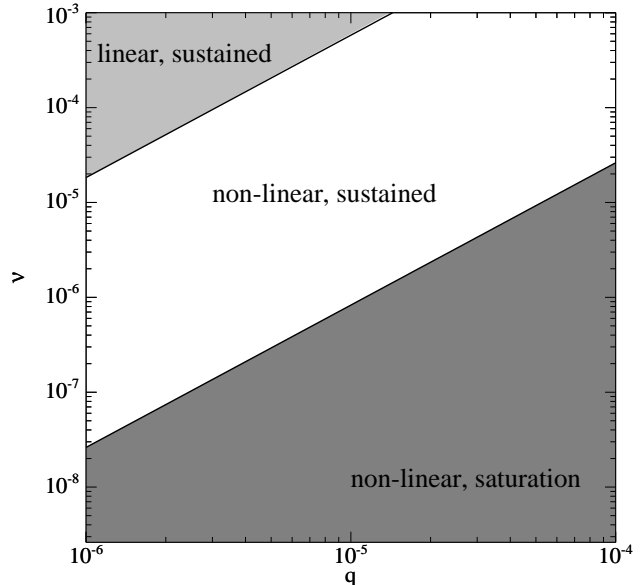


Figure 14. Schematic overview of the different migration regimes. Depending on the magnitude of the viscosity, low-mass planets will either experience a linear, unsaturated torque, a non-linear, unsaturated torque, or a non-linear, saturated torque.

7 DISCUSSION

We have shown that non-linear effects commonly occur in the coorbital region, even for low-mass planets. In inviscid discs, the corotation torque eventually *always* becomes non-linear, saturating after a few libration cycles, so that only the (linear) Lindblad torque survives. Viscosity can prevent the torque from saturating, and for a large enough viscosity, which however decreases with protoplanet mass, the linear torque will be restored. In Fig. 14 we present a schematic overview of the three possibilities in the $(\log q, \log \nu)$ plane. The two lines define the boundaries between the three regions. The boundary between the region where the non linear torque is maintained by viscosity and the saturated regime is given approximately by the condition that viscous diffusion across the coorbital region occurs in one libration cycle. The line separating the sustained horseshoe drag regime from the linear regime is expected to occur where viscous effects become large enough to disrupt horseshoe turns.

Note that the regime for which the corotation torque is linear, occupies only a small fraction of the parameter space. Note also that the borders between the different regions are not razor-sharp. In reality the non-linear torque can be partially saturated, or be reduced by viscosity. However, the overall picture is clear: the corotation torque is almost always non-linear.

For density profiles with close to $\alpha = 3/2$, the non-linear corotation torque, or horseshoe drag, does not play a major role. In an isothermal disc with $\alpha = 1/2$, a commonly adopted value for a locally isothermal disc, the deviation from the linear torque can be up to 30% in the inviscid case (see Fig. 7). If a relatively large viscosity is used, such non-linear behaviour can be markedly reduced (see also the discussion in Paardekooper & Papaloizou 2008). Note also that for a given viscosity, linearity is always restored for small enough protoplanet masses (see Fig. 14). Large

viscosities, numerical and/or imposed, in combination with inadequate numerical resolution for representing horseshoe turns for low-mass planets, conspire to make the non-linear behaviour described here less apparent.

Masset et al. (2006) reported non-linear behaviour for planets of higher mass than considered here, also claimed to be due to the action of the horseshoe drag. However, since the horseshoe width x_s was enhanced relative to its value for low-mass planets, the non-linear torque was much stronger. Masset et al. (2006) define non-linearity as a departure from the torque being proportional to q^2 . In the light of our findings, however, it should be noted that *all* planets in fact show non-linear behaviour in the inviscid limit. For low-mass planets, this non-linearity is less obvious because the horseshoe drag is also proportional to q^2 .

For moderately positive density gradients ($\alpha \leq -1$), the non-linear torque is strong enough to reverse the sign of the total torque. In realistic discs, positive gradients will probably only be realised at special locations, but note that, unlike as was argued in Masset et al. (2006), the gradient does not have to be extremely sharp to stop inward migration. Almost any positive surface density gradient can act as a 'protoplanet trap'.

Barotropic discs with $\alpha < 0$ can also serve as a model for what happens when strong corotation torques arise that are not due to the radial vortensity gradient. In adiabatic discs, for example, there is a strong contribution from any radial entropy gradient (Paardekooper & Mellema 2008; Paardekooper & Papaloizou 2008). Baruteau & Masset (2008) showed that linear theory predicts a contribution from a radial entropy gradient, and argued that this would be strong enough to reverse the total torque. However, Paardekooper & Papaloizou (2008) showed that this linear contribution is in fact small, and that it is a non-linear effect that changes the sign of the torque as observed in Paardekooper & Mellema (2006a), and more recently in Kley & Crida (2008). The non-linear contribution arises in a similar manner to that discussed in this paper (see also Paardekooper & Papaloizou 2008).

We have greatly simplified the problem by keeping the planet on a fixed orbit and choosing the viscosity law such that there is no accretion flow. This way, there is no radial mass flow with respect to the planet. Material that flows past the planet from the inner to the outer disc (or the other way round) exerts an additional torque on the planet (see Masset 2001). The effect of such a radial flow is to introduce an asymmetry in the horseshoe region, which lies at the basis of Type III migration (Masset & Papaloizou 2003). It remains to be investigated how these processes affect the current analysis.

Masset et al. (2006) noted that the effects of non-linearity were much stronger in 3D, probably because the width of the horseshoe region is larger compared to 2D simulations that necessarily have a softening parameter of the order of the scale height of the disc. The full 3D structure of the horseshoe region remains to be investigated, but if the velocity field is essentially two-dimensional, one could regard the vertical structure of the horseshoe region as stacked layers of 2D horseshoes, with a smoothing equal to the vertical distance to the midplane (see also Masset et al. 2006). Then, the term x_s^4 in equation (9) would be replaced by a density-

weighted average (see Masset (2002)):

$$x_s^4 \rightarrow \frac{\int_{-\infty}^{\infty} \rho(r_p, \varphi_p, z) x_s^4(b=z) dz}{\Sigma_p}. \quad (26)$$

However, this procedure requires a proper estimate for x_s for $b \rightarrow 0$, where equation (10) cannot be used. This issue is discussed in a paper.

8 SUMMARY AND CONCLUSION

We have analysed the corotation torque on an embedded planet in a barotropic disc, and shown that this torque is non-linear in general after a few orbits. The linear corotation torque, which is set up on a dynamical time scale, is replaced by horseshoe drag, which is stronger in all cases we have considered. This process completes in approximately one tenth of the libration time scale τ_{lib} or $\sim 2h_p\tau_{\text{lib}}$ in our case.

For discs with large vortensity gradients, a strong departure from linear theory is observed. We have shown that in discs with moderately positive density gradients ($\Sigma \propto r$) non-linear effects can reverse the total torque, leading to outward migration. In particular, this may occur without a very abrupt strong surface density transition of the type considered by ('protoplanetary trap', Masset et al. 2006), and may lead to the halting of the inward migration of low-mass planets.

After one libration time, saturation sets in unless some form of viscosity is able to restore the original density profile within τ_{lib} . For the standard value of $\nu = 10^{-5}$, corresponding to $\alpha_{\text{visc}} = 0.004$, the corotation torque on low-mass planets in the Earth mass range can be sustained by such action.

ACKNOWLEDGEMENTS

We thank W. Kley for useful comments, and the anonymous referee for an insightful report. This work was performed using the Darwin Supercomputer of the University of Cambridge High Performance Computing Service (<http://www.hpc.cam.ac.uk>), provided by Dell Inc. using Strategic Research Infrastructure Funding from the Higher Education Funding Council for England.

REFERENCES

- Baruteau C., Masset F., 2008, ApJ, 672, 1054
- Crida A., Morbidelli A., 2007, MNRAS, 377, 1324
- D'Angelo G., Henning T., Kley W., 2002, A&A, 385, 647
- Goldreich P., Tremaine S., 1979, ApJ, 233, 857
- Goldreich P., Tremaine S., 1980, ApJ, 241, 425
- Kley W., Crida A., 2008, A&A, 487, L9
- Korycansky D. G., Pollack J. B., 1993, Icarus, 102, 150
- Lai D., Zhang H., 2006, MNRAS, 368, 917
- Lin D. N. C., Papaloizou J., 1986, ApJ, 309, 846
- Masset F. S., 2001, ApJ, 558, 453
- Masset F. S., 2002, A&A, 387, 605
- Masset F. S., D'Angelo G., Kley W., 2006, ApJ, 652, 730
- Masset F. S., Morbidelli A., Crida A., Ferreira J., 2006, ApJ, 642, 478

- Masset F. S., Papaloizou J. C. B., 2003, *ApJ*, 588, 494
 Mayor M., Queloz D., 1995, *Nature*, 378, 355
 Nelson R. P., Papaloizou J. C. B., 2004, *MNRAS*, 350, 849
 Ogilvie G. I., Lubow S. H., 2003, *ApJ*, 587, 398
 Paardekooper S.-J., Mellema G., 2006a, *A&A*, 459, L17
 Paardekooper S.-J., Mellema G., 2006b, *A&A*, 450, 1203
 Paardekooper S.-J., Mellema G., 2008, *A&A*, 478, 245
 Paardekooper S.-J., Papaloizou J. C. B., 2008, *A&A*, 485, 877
 Paardekooper S.-J., Papaloizou J. C. B., 2009, *MNRAS*, submitted
 Papaloizou J. C. B., Nelson R. P., Kley W., Masset F. S., Artymowicz P., 2007, in *Protostars and Planets V Disk-Planet Interactions During Planet Formation*. pp 655–688
 Pepliński A., Artymowicz P., Mellema G., 2008, *MNRAS*, 387, 1063
 Tanaka H., Takeuchi T., Ward W. R., 2002, *ApJ*, 565, 1257
 Terquem C. E. J. M. L. J., 2003, *MNRAS*, 341, 1157
 Ward W. R., 1989, *ApJ*, 336, 526
 Ward W. R., 1991, in *Lunar and Planetary Institute Conference Abstracts Horseshoe Orbit Drag*. p. 1463
 Ward W. R., 1992, in *Dermott S. F., Hunter Jr. J. H., Wilson R. E., eds, Astrophysical Disks Vol. 675 of New York Academy Sciences Annals, Disk-Protoplanet Interactions: Torques from the Coorbital Zone*. pp 314–+
 Ward W. R., 1997, *Icarus*, 126, 261
 Ward W. R., 2007, in *Lunar and Planetary Institute Conference Abstracts Vol. 38 of Lunar and Planetary Institute Conference Abstracts, A Streamline Model of Horseshoe Torque Saturation*. p. 2289

APPENDIX

TIME DEVELOPMENT OF THE LINEAR COROTATION TORQUE

We here consider the time development of the linear corotation torque consequent on the insertion of a perturbing protoplanet potential into an unperturbed disc. We specialise to the limit of a low mass planet and adopt a local Cartesian coordinate system (x, y) with origin at the centre of mass of the planet, and the x axis pointing radially outwards. The system rotates uniformly with the Keplerian angular velocity, Ω_p , at the orbital location of the planet. In this frame the differential rotation of the disc is manifest through a linear shear $\mathbf{v} = (v_x, v_y) = (0, -3\Omega_p x/2)$. Thus the background vorticity is constant and the vortensity gradient is proportional to the gradient of $1/\Sigma$.

The governing equations are the inviscid form of the basic equations (1) and (2). As it builds up from nothing, the disc response has to be linear for some period of time after insertion of the protoplanet so we linearise the governing equations treating Φ_p as a linear perturbation. The linear response approaches its final value in a characteristic time independent of the protoplanet mass, in fact we shall see that this is characteristically the orbital time scale. Accordingly a full linear response is guaranteed for a sufficiently small protoplanet mass.

For simplicity we initially discuss the large softening case for which the pressure response is small (see Section 4.3). We then go on to discuss the more general case.

Calculation of the linear response

The linearised forms of the components of (2) in the local system are

$$\frac{Dv'_x}{Dt} - 2\Omega_p v'_y = -\frac{\partial\Phi_{Gp}}{\partial x}, \quad \text{and} \quad (27)$$

$$\frac{Dv'_y}{Dt} + \frac{1}{2}\Omega_p v'_x = -\frac{\partial\Phi_{Gp}}{\partial y}, \quad (28)$$

where perturbation quantities are denoted with a prime and the convective derivative applies to the unperturbed flow such that

$$\frac{D}{Dt} \equiv \frac{\partial}{\partial t} - \frac{3\Omega_p x}{2} \frac{\partial}{\partial y}. \quad (29)$$

These are the local analogues of the global linear equations (12) and (13), Φ_{Gp} here denotes the generalised potential which may be taken to be the sum of the perturbing protoplanet potential and the enthalpy perturbation. For the large softening model, Φ_{Gp} may be taken to be the protoplanet perturbing potential alone. Note we have not made a Fourier decomposition at this point.

We find it convenient to work with the Lagrangian displacement $\boldsymbol{\xi} \equiv (\xi_x, \xi_y)$, which is such that $(v'_x, v'_y) = (D\xi_x/Dt, D\xi_y/Dt + 3\Omega_p \xi_x/2)$. In terms of this (27) and (28) take the form

$$\frac{D^2\xi_x}{Dt^2} - 2\Omega_p \frac{D\xi_y}{Dt} - 3\Omega_p^2 \xi_x = -\frac{\partial\Phi_{Gp}}{\partial x}, \quad \text{and} \quad (30)$$

$$\frac{D^2\xi_y}{Dt^2} + 2\Omega_p \frac{D\xi_x}{Dt} = -\frac{\partial\Phi_{Gp}}{\partial y}, \quad (31)$$

We now perform a Fourier decomposition of Φ_{Gp} in y assuming periodicity on a length scale L_y .

$$\Phi_{Gp} = \mathcal{R}e \sum_{n=0}^{\infty} b_n(x, t) \exp(ink_{y0}y), \quad (32)$$

where $k_{y0} = 2\pi/L_y$ and $\mathcal{R}e$ denotes that the real part is to be taken. We remark that to relate to a full cylindrical annulus, $L_y \rightarrow 2\pi r_p$, $y \rightarrow r_p \varphi$, and $n \rightarrow m$, where m is the usual azimuthal mode number. Using this we obtain

$$\frac{D^2\xi_x}{Dt^2} - 2\Omega_p \frac{D\xi_y}{Dt} - 3\Omega_p^2 \xi_x = -\sum_{n=0}^{\infty} \frac{\partial b_n}{\partial x} \exp(ink_{y0}y), \quad \text{and} \quad (33)$$

$$\frac{D^2\xi_y}{Dt^2} + 2\Omega_p \frac{D\xi_x}{Dt} = -\sum_{n=0}^{\infty} ink_{y0} b_n \exp(ink_{y0}y). \quad (34)$$

In order to solve these equations we make the approximation of neglecting $D^2\xi_x/Dt^2$. This is a common approximation that is made when considering corotation/horseshoe dynamics. It has the effect of removing epicyclic oscillations, and therefore Lindblad torques, but as we shall see it does not interfere with the corotation torque. We then use (33)

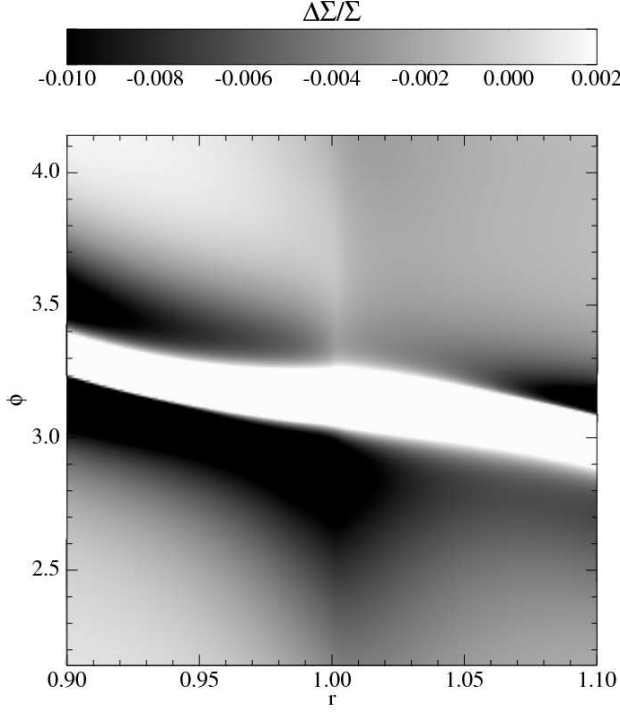


Figure 15. Linear density response for $\alpha = -2$, $b = 0.03$, $h_p = 0.05$ and $q = 1.26 \cdot 10^{-5}$. The color scale has been adjusted to highlight the density ridge at corotation, which gives rise to the linear corotation torque. The planet is located at $r = 1$ and $\phi = \pi$.

to eliminate ξ_x from (34) and thus obtain a second order equation for ξ_y :

$$\frac{1}{3} \frac{D^2 \xi_y}{Dt^2} = - \sum_{n=0}^{\infty} c_n \exp(ink_{y0}y), \quad (35)$$

where

$$c_n = - \frac{2}{3\Omega_p} \frac{\partial^2 b_n}{\partial x \partial t} - ink_{y0}(b_n - xdb_n/dx). \quad (36)$$

This may be integrated to obtain ξ_y and then ξ_x found from the used approximate form of (33). The integration process is aided by noting that $y + 3\Omega_p xt/2$ is invariant under D . Note too that in order to ensure that the boundary condition, that all disturbances vanish at $t = 0$, is satisfied, an appropriate function of $y + 3\Omega_p xt/2$, which plays the role of an integration constant, may be added (D/Dt operating on such a function will be zero). Following the above procedures, which guarantee there will be no singularities in the solution, we obtain

$$\frac{D\xi_y}{Dt} = -3 \sum_{n=0}^{\infty} \exp(ink_{y0}(y + 3\Omega_p xt/2)) \times \int_0^t c_n \exp(-3ink_{y0}\Omega_p xt'/2) dt', \quad (37)$$

$$\xi_x = - \frac{2}{3\Omega_p} \frac{D\xi_y}{Dt} + \frac{1}{3\Omega_p^2} \sum_{n=0}^{\infty} \frac{db_n}{dx} \exp(ink_{y0}y) \quad (38)$$

and

$$\xi_y = -3 \sum_{n=0}^{\infty} \exp(ink_{y0}(y + 3\Omega_p xt/2)) \times \int_0^t c_n \exp(-3ink_{y0}\Omega_p xt'/2) (t - t') dt'. \quad (39)$$

We note that in the above and other similar integrands, unless otherwise indicated, quantities are evaluated at the time t' . We may now find the density perturbation (see Fig. 15 for and example) from

$$\Sigma' = -\nabla \cdot \Sigma \xi \quad (40)$$

and then evaluate the corotation torque acting on the planet, $\Gamma_{c,\text{lin}}$, by doing the torque integral

$$\Gamma_{c,\text{lin}} = r_p \int \mathcal{R}e(\Sigma') \mathcal{R}e\left(\frac{\partial \Phi_{\text{GP}}}{\partial y}\right) dx dy, \quad (41)$$

where we have adopted a multiplicative factor equal to an orbital radius r_p in order to convert a force in the y direction into a torque. Substituting the Fourier expansion of $\partial \Phi_{\text{GP}}/\partial y$ and integrating over y we find, after some elementary algebra, that $\Gamma_{c,\text{lin}} = \Gamma_a + \Gamma_b$, where

$$\Gamma_a = \frac{2\pi}{\Omega_p} \sum_{n=0}^{\infty} \int_{-\infty}^{\infty} \int_0^t \frac{d(\Sigma d_n)}{dx} n^2 b_n \cos \chi_n(x, t') dt' dx, \quad (42)$$

with $\chi_n(x, t') = 3nk_{0y}\Omega_p x(t - t')/2$, and

$$\Gamma_b = \frac{2\pi r_p}{\Omega_p} \sum_{n=0}^{\infty} \int_{-\infty}^{\infty} \int_0^t \frac{d(\Sigma f_n)}{dx} n b_n \sin \chi_n(x, t') dt' dx, \quad (43)$$

with $d_n = b_n - x \partial b_n / \partial x$, and $f_n = (2/3\Omega_p) \partial^2 b_n / \partial x \partial t'$.

The expression for Γ_b can be integrated by parts with respect to t' and combined with that for Γ_a to yield the following expression for the total torque:

$$\Gamma_{c,\text{lin}} = \frac{2\pi}{\Omega_p} \sum_{n=0}^{\infty} \int_{-\infty}^{\infty} \int_0^t \frac{d\Sigma}{dx} n^2 b_n^2 \cos \chi_n(x, t') dt' dx. \quad (44)$$

Equation (44) shows how the corotation torque develops with time after a protoplanet is inserted at $t = 0$. We shall see that this is on the time scale of the orbital period. Consider first the case when the b_n are independent of time as would be the case for a large softening length compared to the scale height where there is negligible pressure response. Then the integral with respect to t' can be performed with the result that

$$\Gamma_{c,\text{lin}} = \frac{4\pi r_p}{3\Omega_p^2} \int_{-\infty}^{\infty} \sum_{n=0}^{\infty} n g_n(x = \zeta L_y / (3n\pi\Omega_p t)) \frac{\sin \zeta}{\zeta} d\zeta, \quad (45)$$

where $g_n(x) = b_n(x)^2 (d\Sigma/dx)$.

We remark that most of the contribution to the integral comes from $\zeta \sim 1$. The corresponding value of $x \sim L_y / (3n\pi\Omega_p t) \sim 2r_p / (3n\Omega_p t)$. Thus at early times the corotation torque has contributions from mainly large radii but as time progresses the contributing region contracts towards the corotation circle. To estimate the time involved, we note that for large softening, the value of n giving the dominant

Fourier components for the corotation torque is expected to be $n \sim 1/b$, with contributions from larger values of n being reduced because of smoothing. We then see that the region contributing to the corotation torque is within br_p of the corotation circle within an orbital period independently of its size. Thus the linear corotation torque in this model is established in about an orbital period.

The limiting value is easily obtained by letting $t \rightarrow \infty$ in the above expression. The result after performing the integration is

$$\Gamma_{c,\text{lin}} = \frac{4\pi^2 r_p}{3\Omega_p^2} \sum_{n=0}^{\infty} nb_n(0)^2 (d\Sigma/dx)_{x=0}. \quad (46)$$

This is exactly what is obtained from the expression (4) given by Goldreich & Tremaine (1979) recalling that the vorticity in the background local model is constant and equal to $\Omega_p/2$ making the vortensity gradient proportional to the gradient of $1/\Sigma$. To illustrate the density response in the neighbourhood of corotation we plot the linear surface density response for the case with $\alpha = -2$, $b = 0.03$, $h_p = 0.05$ and $q = 1.26 \cdot 10^{-5}$ in figure 15. This was calculated following the procedure described in section 4. In addition to the strong wake produced by the Lindblad torques there is both an overdensity leading and an underdensity trailing the planet. These narrow features are localized on the corotation circle as expected from the analysis presented here. These produce a positive torque acting on the planet.

Although (46) has been obtained assuming the softening length is large compared to the scale height, we expect it to apply more generally. When the softening parameter is not large and the generalised potential, Φ_{G_p} is used, the added enthalpy perturbation results in the b_n being unknown functions of time. However, the linear response calculation of Goldreich & Tremaine (1979) indicates that the scale of the response is $|x| \sim H$, with the dominant values of $n \sim r_p/H$. Equation (44) then indicates only values of $|t - t'| < \sim r_p/(nH\Omega_p) \sim \Omega_p^{-1}$ will contribute significantly to the torque. Thus when Φ_{G_p} varies slowly compared to the orbital period, expected as the linear response approaches its steady value, b_n may be taken to be locally constant in time, and then from the above discussion, the corotation torque will be the local Goldreich & Tremaine (1979) value. The situation is also similar at early times. For $t < \sim r_p/(nH\Omega_p) \sim \Omega_p^{-1}$, the cosine term in equation (44) may be replaced by unity. This then implies that at early times

$$\Gamma_{c,\text{lin}} = \frac{4\pi^2 r_p}{3\Omega_p^2} \sum_{n=0}^{\infty} \frac{3nH\Omega_p t}{\pi r_p} \left\langle \frac{d\Sigma}{dx} nb_n^2 \right\rangle, \quad (47)$$

where the angled brackets denote an appropriate integral mean. When t approaches Ω_p^{-1} , this becomes the same mean of torques of the form (4).

Note that the time to establish the linear response and corotation torque, the latter expected to be finite, does not depend on the size of the perturbation, or accordingly, q . This time should be an intrinsic time which can only be a multiple of the orbital period. Accordingly for sufficiently small q we can ensure that the system is in the linear regime when the torque is set up so that the linear formulation should be valid then.